Interlayer microstructure of sputtered Mo/Si multilayers

1997 J. Phys.: Condens. Matter 9 3521

(http://iopscience.iop.org/0953-8984/9/17/003)

J. Phys.: Condens. Matter **9** (1997) 3521–3528. Printed in the UK PII: S0953-8984(97)76330-6

Interlayer microstructure of sputtered Mo/Si multilayers

Liwen Wu†, Shiqiang Wei†, Bing Wang† and Wenhan Liu‡

† Centre for Fundamental Physics, University of Science and Technology of China, Hefei 230026, People's Republic of China

‡ Department of Physics, and Structure Research Laboratory, University of Science and Technology of China, Hefei 230026, People's Republic of China

Received 16 July 1996, in final form 2 January 1997

Abstract. K-edge transmission-mode extended x-ray absorption fine structure, transmission electron microscopy, and x-ray diffraction have been used to investigate the microstructure of Mo/Si multilayers with periods ranging from 20 to 2.0 nm (the layer thickness ratios of Mo to Si were 1:2). The results confirmed that there was a Mo–Si amorphous interlayer between the Mo and Si layers, the Mo–Si coordination was about 80% in the first shell neighbouring the Mo atom in the interlayer, and the total coordination number was 7.4, approximately equal to that of bcc Mo. A thermally activated model is suggested as a basis for explaining the interlayer formation mechanism by considering the different thermal conductivities of the deposited Mo and the amorphous Si surfaces.

1. Introduction

In recent years, much attention has been given to the stability [1–3] and optical performance for wavelengths ranging from 12 to 25 nm [4–8] of periodic Mo/Si multilayers. The microstructure of the Mo/Si system has also been widely studied [9–20]. High-resolution transmission electron microscopy (HRTEM), Auger electron spectroscopy (AES), and Rutherford backscattering spectroscopy (RBS) have revealed that there is an interlayer between the Si and Mo layers, but its microstructure and the formation mechanism (thermally activated [9], or via energetic adatom (especially Mo atom) penetration [10, 21]) are still not clear. Extended x-ray absorption fine structure (EXAFS), which is caused by the coherence of outgoing and backscattered photoelectron waves, is useful as a basis for measurements of the neighbourhood of absorbing atoms. In this work, we have focused on the interlayer microstructure in sputtered Mo/Si multilayers and its formation mechanism. For this purpose, the EXAFS, transmission electron microscopy (TEM), and low-angle x-ray diffraction (LAXRD) techniques were used to study the local environment of Mo atoms in Mo/Si multilayers with periods ranging from 20 to 2.0 nm.

2. Experiment

The Mo/Si multilayers were fabricated by magnetron sputtering. Alternating layers of elemental molybdenum (purity 99.99%) and silicon (purity 99.999%) were deposited under an rf-powered Si target and a dc-powered Mo target. The base vacuum and sputtering argon pressures were 10^{-4} Pa and 1.00 Pa, respectively. The sputtering pressure was not the optimal pressure for making high-quality Mo/Si multilayers [8], but it was the optimal

0953-8984/97/173521+08$19.50

pressure for controlling deposition in our apparatus. Since an adequate amount of film must be deposited to make EXAFS samples, the stability of the deposition apparatus is important. The deposition rates, which were obtained from the ratios of layer thicknesses of Si and Mo (about 200 nm, measured by an interference microscope) to the deposition time, were 3.2 nm min^{-1} and 2.7 nm min^{-1}, respectively.

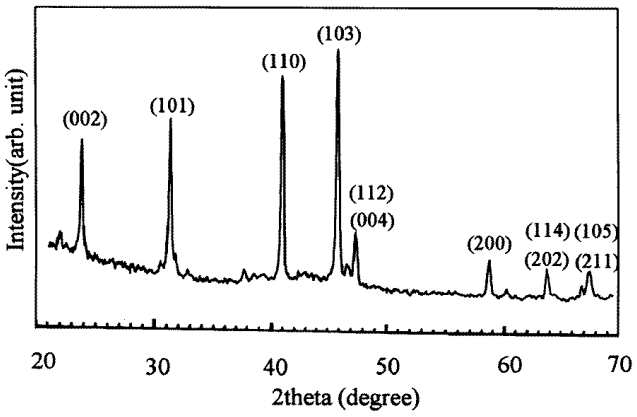

Figure 1. The XRD pattern of the model compound $MoSi_2$. The intensities are almost the same as on the JCPDS card.

The nominal periods (thicknesses of Mo/Si bilayers) of the Mo/Si multilayers for the EXAFS measurements were 20, 5.0, and 2.0 nm, and their layer thickness ratios of Mo to Si were 1:2. A 10 nm sputtered Si buffer layer was deposited between the multilayer and the glass substrate in each sample. A Mo film 300 nm thick was also prepared for comparison. To obtain a high signal–noise ratio, the EXAFS data were collected in the transmission mode, so the glass substrates had to be removed. After the LAXRD experiment, each sample was peeled off its glass substrate with adhesive tape, and then was cut into several strips, and stacked to obtain the optimal thickness (thicker than one absorption length). Two model compounds, Mo powder and crystalline $MoSi_2$ (c-$MoSi_2$), were prepared to obtain the backscattering amplitudes and phase shifts of Mo–Mo and Mo–Si atom pairs to which to fit the EXAFS data. The Mo powder was filed from a block of metallic Mo. The c-$MoSi_2$ sample was prepared by annealing a Mo/Si multilayer sample. The XRD showed that the annealed sample was c-$MoSi_2$ (6U) (figure 1). The LAXRD was carried out in a Rigaku D10-C diffractometer. The Mo K-edge EXAFS spectra of the samples were measured at the XAFS station of the 4W1B beamline, Beijing Synchrotron Radiation Facility (BSRF). Si(111) double crystals were used as the monochromator. Data were collected by two ion chambers filled with argon at room temperature. The energy resolution was about 2 eV as judged from the Cu foil 3d near-edge feature.

The TEM samples were deposited on newly cleaved NaCl crystals in the same conditions as those for the EXAFS samples. There was also a 10 nm Si buffer layer between the Mo/Si multilayer and the substrate in each sample, to eliminate the effect of using a different kind of substrate. The period numbers of the samples with periods of 20, 5.0, and 2.0 nm were 2, 8, and 20, respectively; thus their total thicknesses were almost the same. After being taken from the NaCl crystals, these samples were examined in a Hitachi H-800 transmission electron microscope operated at 200 kV.

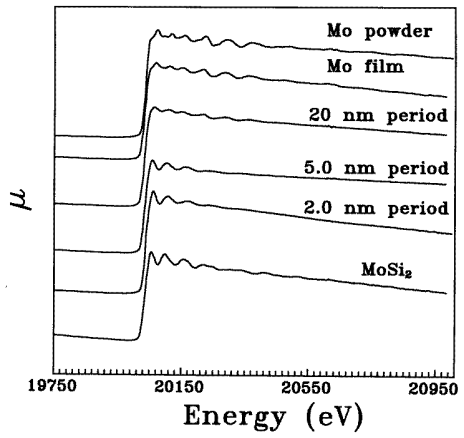

Figure 2. Mo K-edge absorption spectra of the samples.

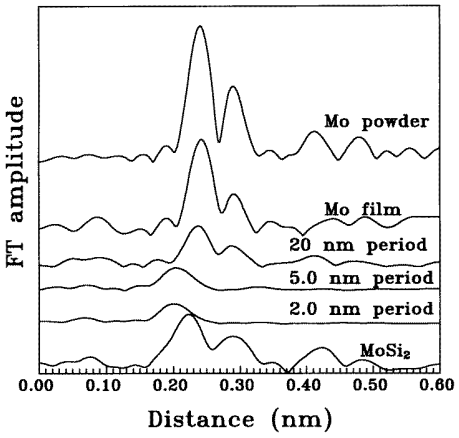

Figure 3. The Fourier transforms of $\chi(\boldsymbol{k})k^3$ for the samples.

3. Results and discussion

The Mo K-edge absorption spectra of the samples are shown in figure 2.

From the absorption spectra, we can get the normalized absorption oscillation $\chi(\boldsymbol{k})$:

$$\chi(\boldsymbol{k}) = \frac{\mu - \mu_0}{\mu_0} \tag{1}$$

where $\boldsymbol{k}$ is the wavevector of the photoelectron, μ is the absorption coefficient, and μ_0 is the absorption coefficient of the isolated atom.

Generally, the EXAFS oscillation function can be described as [24–27]

$$\chi(k) = \sum_j \frac{N_j F_j(k) S_0^2(k)}{kR_j^2} \exp(-2\sigma_j^2 k^2) \exp[-2R_j/\lambda(k)] \sin[2kR_j + \delta_j(k)] \tag{2}$$

where N_j is the number of atoms in the jth shell, R_j is the mean distance between the absorbing atom and the jth shell, $F_j(\boldsymbol{k})$ is the magnitude of the backscattering amplitude of the jth-shell atoms, $S_0^2(\boldsymbol{k})$ is about 0.7 to 0.9 [28, 29] and is caused by many-body effects and dynamic relaxation (it is usually used together with $F_j(\boldsymbol{k})$ in data fitting), $\lambda(\boldsymbol{k})$ is the mean free path of the photoelectron [30], $\delta_j(\boldsymbol{k})$ is the electronic phase shift, and σ_j is the root mean square disorder of the absorbing atom and atoms in the jth shell, including both static and thermal contributions.

For large-disorder samples, considering the first shell only, the EXAFS oscillation function should be expressed as [31, 32]

$$\chi(\boldsymbol{k}) = \frac{N_1 F(\boldsymbol{k}) S_0^2(\boldsymbol{k})}{kR^2(1 + 4k^2\sigma_s^2)^{1/2}} \exp(-2\sigma_t^2 k^2) \exp[-2R/\lambda(\boldsymbol{k})] \times \sin[2kR + \delta(\boldsymbol{k}) + \arctan(2k\sigma_s) - 2k\sigma_s] \tag{3}$$

where N_1 is the coordination number of the first shell, R is the mean distance between the absorbing atom and the first shell, σ_s is the root mean square structural (static) disorder, and σ_t is the thermal disorder factor.

The Fourier transform (FT) of $\chi(\boldsymbol{k})k^3$ is shown in figure 3. The total range of k is 25 to 150 nm^{-1} in the FT. The strong peaks for Mo powder at 0.240 and 0.290 nm are

Table 1. The best fitting parameters for the samples, where R is the mean distance between the absorbing atom and the scattering atom, s is the disorder factor, N is the coordination number, and p is the percentage of each kind of bond.

	The first shell					The second shell				
Sample	Pair	R (nm)	s (nm)	N	p	Pair	R (nm)	s (nm)	N	p
Mo powder	Mo–Mo	0.272	0.0052	8.0	100	Mo–Mo	0.314	0.0065	6.0	100
300 nm Mo film	Mo–Mo	0.273	0.0065	7.9	100	Mo–Mo	0.317	0.0070	4.5	100
Mo/Si with	Mo–Mo	0.271	0.0091	6.2	84					
20 nm period	Mo–Si	0.260	0.0065	1.2	16					
Mo/Si with	Mo–Mo	0.270	0.0120	1.6	22					
5.0 nm period	Mo–Si	0.261	0.0150	5.8	78					
Mo/Si with	Mo–Mo	0.269	0.0120	1.5	20					
2.0 nm period	Mo–Si	0.260	0.0158	6.0	80					
$MoSi_2$ (6U)	Mo–Si	0.262	0.0054	10.0	100	Mo–Mo	0.320	0.0059	4.0	100

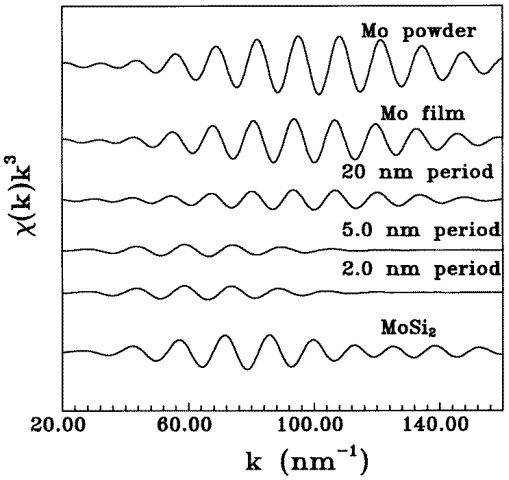

Figure 4. The inverse transformation for the first coordination peak of the FT.

contributed by the first shell (the standard bond length $R = 0.272$ nm; coordination number $N = 8$) and the second shell ($R = 0.314$ nm, $N = 6$), respectively. By comparison with the standard values, we can get the phase shift and backscattering amplitude of the Mo–Mo pair from the powder of the model compound Mo and those for the Mo–Si pair from the c-$MoSi_2$sample. The FT features for the 300 nm Mo film are similar to those for the Mo powder. For the Mo/Si multilayer with the period 20 nm, the amplitudes of the first and the second peak decrease drastically compared with those for the Mo powder, but their peak positions remain the same. There are similar FT profiles for Mo/Si with the periods 2.0 and 5.0 nm (only one weak peak appears at a distance 0.200 nm), but these are clearly different to that for the Mo/Si multilayer with the period of 20 nm. The distance of the

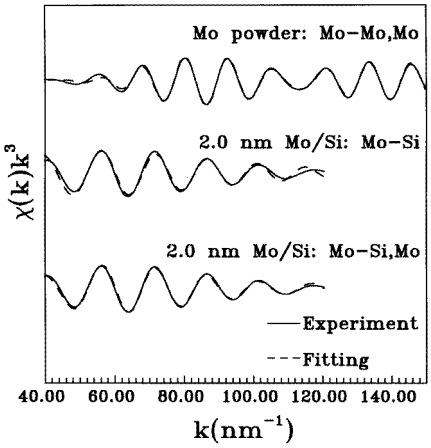

Figure 5. The fits of the EXAFS spectra.

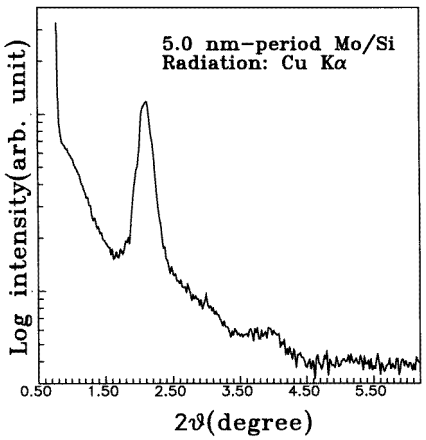

Figure 6. The LAXRD pattern of a Mo/Si multilayer with the nominal period 5.0 nm. The period calculated (taking refractive collection into consideration) from the peak position is 4.39 nm.

peak is 0.040 nm less than that of the first coordination shell for Mo powder and 0.024 nm less than that for $MoSi_2$. So we see that the Mo/Si samples with periods of 2.0 and 5.0 nm are amorphous.

The amplitude function contains information on the kind and number of the scattering atoms: the strong oscillation of the light element is mainly in the low-k region and that of the relatively heavy element is in the high-k region [34]. In order to get more detailed structural information, the inverse transformation is performed for a selected peak of the FT. Figure 4 shows the inverse transformation results for the first peak of figure 3. The strong oscillatory peaks in the high-k region are mainly contributed by the Mo–Mo coordination, and those in the low-k region are mainly contributed by the Mo–Si coordination. The inverse transform profiles of the Mo/Si samples with periods of 2.0 and 5.0 nm resemble that of c-$MoSi_2$, except as regards the significant extinction of the oscillatory amplitude in the high-k region. Such results reveal that the Mo atom is mainly coordinated by Si atoms

in the first shell in these two samples. The structural parameters of the Mo/Si multilayer with the period 20 nm and the Mo film were fitted with equation (2), and the large-disorder Mo/Si samples with the periods 2.0 and 5.0 nm were analysed using equation (3). The fits of the EXAFS spectra are shown in figure 5. The best fitting parameters are shown in table 1.

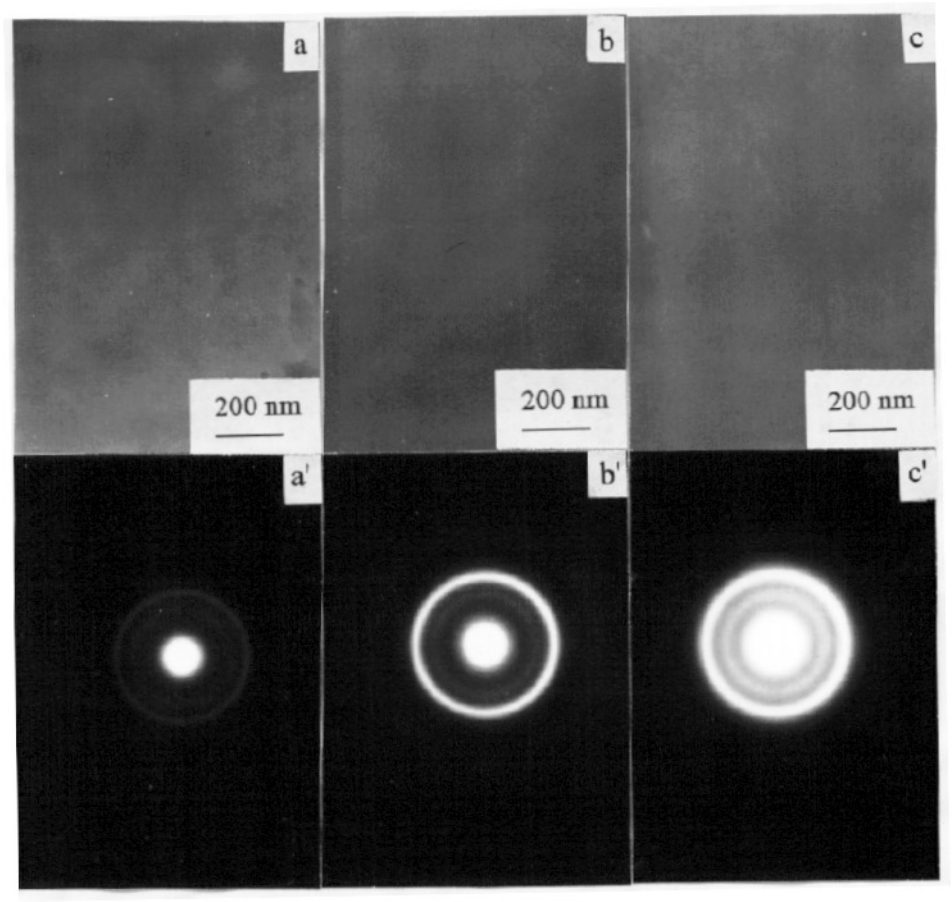

Figure 7. The TEM morphological images and SAED patterns for the Mo/Si multilayers with the periods of 20 nm ((a), (a′)), 5.0 nm ((b), (b′)), and 2.0 nm ((c), (c′)). As the period decreases, the diffuseness of the diffraction rings increases.

The LAXRD patterns of the Mo/Si multilayers with the periods 20 and 5.0 nm indicated that they are periodic. The LAXRD pattern of the Mo/Si multilayer with the period 5.0 nm is shown in figure 6. No LAXRD peak was found for the sample with the period of 2.0 nm; this suggested that it was non-periodic within our experimental precision.

There are 16% Si coordinations in the first shell of Mo in the sample with the period 20 nm. This means that the Mo–Si interface is not atomically abrupt. There should be a mixed interlayer between the Mo and Si layers. The thinner the layers, the larger the ratio of interlayer to period. Since the Mo neighbourhoods in the samples with the periods 5.0 and 2.0 nm were almost the same, and the LAXRD showed that the former was periodic but the latter was non-periodic, the Mo atom local structure of the sample with the period 2.0 nm

could be considered that of the interlayer. The total coordination numbers of the first shells of the Mo/Si multilayers with the periods 20 nm (Mo–Mo coordination dominant), and 2.0 and 5.0 nm (Mo–Si coordination dominant) are nearly the same (about 7.4), approximately equal to that of bcc Mo.

The TEM morphological images of the Mo/Si samples show uniform contrasts (figures 7(a), 7(b), 7(c)), but their selected-area electron diffraction (SAED) patterns are different: as the period decreases, the diffuseness of the diffraction rings clearly increases (figures 7(a′), 7(b′), 7(c′)). The SAED patterns of the samples with periods of 5.0 and 2.0 nm are different even though their Mo local environments are similar. So some of their local environments, e.g., the Si–Si coordination, must be different.

If the interlayer was formed by the adatoms penetrating the deposition surface (especially Mo atoms penetrating Si), the Mo coordination should be sensitive to the layer thickness and adatom energy. But the interlayers could be found in both electron-beam evaporation (typical adatom energy: 0.1 eV) and sputtering (typical adatom energy: higher than 1 eV) [9–11]. This conclusion of thickness sensitivity is also in conflict with our EXAFS results. After considering all of the above, we conclude that the formation of the interlayer should be thermally activated. Xiu [35] had observed the island-like growth characteristic of the beginning of Mo-on-Si deposition by TEM. Because the thermal conductivity of Mo is higher than that of amorphous Si, when Si atoms are deposited on a Mo surface, the heat produced by the adatoms will diffuse quickly, and the local temperature will be lower than that for the Mo-on-Si process, so the diffusion is less likely to happen in the Si-on-Mo case. This will lead to a thinner interlayer for Si-on-Mo deposition compared with that for the Mo-on-Si case [1, 9, 10]. The mean temperature of the whole sample is usually not higher than 300 °C during sputtering deposition [36], and not much lower than the composition temperature of the first phase $MoSi_2$ (6U) of the Mo–Si system (525 °C [37]), so amorphous Mo–Si does not crystallize during deposition.

4. Conclusion

It has been found that there is a Mo–Si amorphous interlayer between Mo and Si layers. The first-shell total coordination number of the Mo atom neighbourhood was about 7.4. The interlayer formation process was mainly thermally activated. The difference in thickness between the Mo-on-Si interlayer and the Si-on-Mo interlayer was caused by the different thermal conductivities of the surfaces deposited (Mo and amorphous Si).

Acknowledgments

We would like to thank Dr Xin Ju and Dr Bin Lu for their help in doing the EXAFS and TEM experiments. We also thank the Beijing Synchrotron Radiation Facility for giving us the beamtime for the EXAFS measurement. This work was partially supported by the National Natural Science Foundation of China.

References

[1] Barbee T W Jr, Rife J C, Hunter W R, Kowalski M P, Cruddace R G and Seely J F 1993 *Appl. Opt.* **32** 4852
[2] Jiang Z M, Jiang X M, Liu W H and Wu Z Q 1989 *J. Appl. Phys.* **65** 196
[3] Kondratenko V V, Pershin I P and Poltseva O V 1993 *Appl. Opt.* **32** 1811
[4] Barbee T W Jr, Mrowka S and Hettrick M C 1985 *Appl. Opt.* **24** 883
[5] Stearns D G, Rosen R S and Vernon S P 1993 *Appl. Opt.* **32** 6952

[6] Vernon S P, Stearns D G and Rosen R S 1993 *Appl. Opt.* **32** 6969
[7] Slaughter J M, Schulze D W, Hills C R, Mirone A, Stalio R, Watts R N, Tarrio C, Lucatorto T B, Krumrey M, Mueller P and Falco C M 1994 *J. Appl. Phys.* **76** 2144
[8] Slaughter J M and Falco C M 1992 *Nucl. Instrum. Methods Phys. Res.* A **319** 163
[9] Stearns M B, Chang C-H and Stearns D G 1992 *J. Appl. Phys.* **71** 187
[10] Petford-Long A K, Stearns M B, Chang C-H, Nutt S R, Stearns D G, Ceglio N M and Hawryluk A M 1987 *J. Appl. Phys.* **61** 1422
[11] Slaughter J M, Shapiro A, Kearney A K and Falco C M 1991 *Phys. Rev.* B **44** 3854
[12] Montcalm C, Sullivan B T, Pepin H, Dobrowolski J A and Sutton M 1994 *Appl. Opt.* **33** 2057
[13] Rosen R S, Stearns D G, Viliardos M A, Kassner M E, Vernon S P and Cheng Y 1993 *Appl. Opt.* **32** 6975
[14] Takenaka H, Kawamura T, Ishii Y and Asagiri S 1995 *J. Appl. Phys.* **78** 5227
[15] Hunter W R and Seely J F 1993 *Appl. Opt.* **32** 4846
[16] Holloway K, Do K B and Sinclair R 1989 *J. Appl. Phys.* **65** 74
[17] Meyerheim H L, Dößler U, Puschmann A and Baberschke K 1990 *Phys. Rev.* B **41** 5871
[18] Gaines D P, Spitzer R C, Ceglio N M, Krumrey M and Ulm G 1993 *Appl. Opt.* **32** 6991
[19] Bender H A, Silfvast W T, Beck K M and Singh R K 1993 *Appl. Opt.* **32** 6999
[20] Windt D L, Waskiewicz W K and Griffith J E 1994 *Appl. Opt.* **33** 2025
[21] Morgan W L and Boercher D B 1991 *Appl. Phys. Lett.* **59** 1176
[22] Baglin J E E, d'Heurle F M, Hammer W M and Petersson S 1980 *Nucl. Instrum. Methods* **168** 491
[23] Yanagisawa S and Fukuyama T 1980 *J. Electrochem. Soc.* **127** 1150
[24] Stern E A, Sayers D E and Lytle F W 1975 *Phys. Rev.* B **11** 4836
[25] Lytle F W, Sayers D E and Stern E A 1975 *Phys. Rev.* B **11** 4825
[26] Sayers D E and Bunker B A 1988 *X-ray Absorption: Principles, Applications, Techniques of EXAFS, SEXAFS and XANES* ed D C Koningsberger and R Prins 1988 (New York: Wiley) p 211
[27] Crozier E D, Rehr J J and Ingalls R 1988 *X-ray Absorption: Principles, Applications, Techniques of EXAFS, SEXAFS and XANES* ed D C Koningsberger and R Prins 1988 (New York: Wiley) p 373
[28] Stern E A *et al* 1983 Basic principles and applications of EXAFS *Handbook on Synchrotron Radiation* vol 11, ed E E Kock (Amsterdam: North-Holland)
[29] Li H F 1993 *MSc Dissertation* Physics Institute of the Academia Sinica (in Chinese)
[30] Teo B K 1981 *J. Am. Chem. Soc.* **103** 3990
[31] Finney J L 1970 *Proc. R. Soc.* A **319** 479
Finney J L 1977 *Nature* **266** 309
[32] De Crescenzi M, Balzarotti A, Comin F, Incoccia L, Mobilio S and Motta N 1983 *Solid State Commun.* **37** 921
[33] Lee P A, Citrin P H, Eisenberger P and Kincaid B M 1981 *Rev. Mod. Phys.* **53** 769
[34] Lee P A and Beni G 1977 *Phys. Rev.* B **15** 2862
[35] Xiu L S 1992 *PhD Thesis* University of Science and Technology of China (in Chinese)
[36] Naeem M D and Chidambarrao D 1995 *Appl. Phys. Lett.* **66** 2472
[37] Poate J M, Tu K N and Mayer J W (ed) 1978 *Thin Film Interdiffusion and Reactions* (New York: Wiley) ch 12